SEISMIC FRAGILITY ASSESSMENT OF BUILDING-TYPE STRUCTURES IN OIL REFINERIES

A. K. Kazantzi[1*], **N. D. Karaferis**[2], **V. E. Melissianos**[3], **K. Bakalis**[4] and **D. Vamvatsikos**[5]

[1]*Senior Risk Engineer, Resilience Guard GmbH, Steinhausen, Switzerland.*

[2]*Ph.D. Candidate, School of Civil Engineering, National Technical University of Athens, Athens, Greece.*

[3]*Research Associate, School of Civil Engineering, National Technical University of Athens, Athens, Greece.*

[4]*Research Associate, School of Civil Engineering, National Technical University of Athens, Athens, Greece.*

[5]*Associate Professor, School of Civil Engineering, National Technical University of Athens, Athens, Greece.*

Keywords: oil refinery; critical infrastructure; seismic fragility; buildings.

Abstract. *A seismic fragility assessment methodology is presented for equipment-supporting reinforced concrete and steel buildings that are typically encountered in oil refineries. Using a suite of hazard-consistent ground motions and reduced-order models, incremental dynamic analysis is performed to obtain the seismic demand of the structural systems examined. Appropriate drift- and floor acceleration-sensitive failure modes are considered to define the limit state capacities of the supporting structure and the nested non-structural process equipment. Special care is exercised on the demand and capacity representation of structural and non-structural components, offering a transparent roadmap for undertaking analytical fragility assessment for equipment-supporting buildings typical to an oil refinery. The findings and the proposed methodology can be exploited by designers and facility managers for mitigating the risk of failure prior to the occurrence of an earthquake event, for designing the pertinent structures and their non-structural components by means of a risk-aware performance-based methodology, or as feed data in early warning systems.*

1 INTRODUCTION

Oil refineries employ a wide spectrum of structural systems to deliver products that are vital to the economy and society. The structural stock in typical crude oil refineries comprises: (1) flare stacks, i.e. combustion devices at the top of a steel lattice tower that burn any unwanted gases produced during the refining process; (2) reinforced concrete and/or steel chimneys for the release of non-toxic gaseous wastes; (3) pipe-racks that support piping and vessels at single or multiple levels; (4) atmospheric tanks for the storage of liquid-form products; (5) pressurised vessels for the storage of gas products; (6) open-frame steel and/or reinforced concrete buildings that support process equipment, such as pressure vessels, heat exchangers, pumps, reactors, vacuum chargers, converters, and electrical equipment (Sullivan *et al*. 2015).

Owing to the hazardous materials that are processed in a refinery, design codes aim to ensure the structural and operational integrity of the refinery assets against natural hazards. However, despite the strict criteria enforced in the design of their assets, the so-called natural-technological (NaTech) accidents still occur at refineries (e.g., Godoy 2007; Hatayama 2008; Girgin 2011; Bi *et al*. 2021; Krausmann and Cruz 2021), highlighting the need to: (1)

[*] Corresponding author: nancy.kazantzi@resilienceguard.ch

conceptually revisit the way oil refineries are designed; (2) explicitly tailor them to comply with an acceptable pre-defined risk of failure (e.g., Franchin *et al*. 2018; Vamvatsikos *et al*. 2020; Kazantzi and Vamvatsikos 2021); and (3) develop an accurate, yet easy to implement, performance-based methodology (Cornell and Krawinkler 2000) for assessing their risk and resilience against future events. The latter is crucial for operators and stakeholders since it will eventually improve the post-event response efficiency and the pertinent action protocols, enhance business continuity planning, and result in more informed pre-event mitigation actions, allowing also for the consideration of potential cascading effects.

Research to date on the seismic fragility of oil refinery structures is unevenly distributed among them. While liquid storage tanks (e.g., Bakalis *et al*. 2017; Spritzer and Guzey 2017; Vathi *et al*. 2017; Phan *et al*. 2020; Bakalis and Karamanos 2021; Caprinozzi and Dolšek 2021; Hernandez-Hernandez *et al*. 2021; Yu and Whittaker 2021), pipe-racks (e.g., Bursi *et al*. 2018; Di Sarno and Karagiannakis 2020; Farhan and Bousias 2020; Zhang *et al*. 2021) and pressure vessels (e.g., Patkas and Karamanos 2007; Karakostas *et al*. 2015; Fiore *et al*. 2018) are considered well-studied, flare stacks, chimneys (e.g. Guo and Zhang 2019), piping systems within plants (Bursi *et al*. 2015; Di Sarno and Karagiannakis 2020) and open-frame structures (e.g., Butenweg *et al*. 2021) have received comparatively little attention. With regards to the process equipment nested in industrial frame structures, literature is again scarce (e.g., Merino Vela *et al*. 2019), while on-ground supported equipment, such as transformer bushings (e.g., Brennan and Koliou 2020) or vessels founded at the ground level, are more widely studied and documented (Diamanti *et al.* 2011; Wieschollek *et al.* 2013; Korndörfer *et al*. 2017). Further to the above, the financial estimates of past earthquakes in highly industrialised countries have revealed that the losses associated with damage in the critical nested equipment are likely to exceed those in the supporting structures by several orders of magnitude (Butenweg and Holtschoppen 2013). Such losses are often aggravated by the shutdown and the potential release of hazardous materials that could lead to fire, explosion, and contamination, even beyond the boundaries of the refinery.

When available, data from past earthquake events that affected industrial plants (e.g., Sezen and Whittaker 2006; Hatayama 2015), could be utilised for undertaking a seismic vulnerability assessment in industrial facilities. Based on such data, one may define seismic fragilities for individual assets or classes of assets with similar key features. However, such data remain sparse, while they are subject to well-known deficiencies, such as the subjectivity related to the damage assessment, the discrepancies in the structural health of assets (due to maintenance or deterioration) at the time of the earthquake, and the inhomogeneous structural responses due to the lack of a set of representative (index) structures for each characteristic asset class (Iervolino *et al*. 2004).

Owing to the above, this study is built upon an analytical context for deriving seismic fragility curves for the industrial building-type assets of interest supporting several non-structural components (industrial equipment). Seismic damages are accounted for both the supporting structure as well as its non-structural components, including nested industrial equipment and other drift-sensitive attachments. Therefore, a set of reinforced concrete and steel structures—typical to an oil refinery—that support a variety of process equipment was considered. The selected buildings were assumed to have floor slabs with considerable mass and in-plane rigidity as well as substantial overstrength. This is deemed to be the typical case for equipment-supporting structures in oil refineries, due to the strict deformation and fire-design requirements. The nested equipment was also assumed to be typical in terms of type, location, mass and overstrength of its anchorage. It should be pointed out that, each oil refinery has its own distinct characteristics. Hence, our intention was primarily to capture general building/content morphologies that are indicative of oil refineries in order to serve the needs of demonstrating our analytical seismic fragility assessment approach, in a way that can be easily

adapted to the particularities of other refinery plants. For each one of these assets, analytical structural and non-structural seismic fragility curves were computed that could be readily exploited in a seismic risk-aware framework for either performing a more efficient design or a rapid damage assessment for the industrial assets of interest. Overall, this study will eventually offer a transparent roadmap for undertaking an analytical seismic fragility assessment for typical equipment-supporting structures in oil refineries, accounting for all kind of structural, as well as drift- or acceleration-sensitive nonstructural elements. The proposed pathway is paved in a manner that allows its direct integration into a seismic risk assessment model that accounts for all the important structures (e.g. high-rise stacks; liquid storage tanks) in an oil refinery plant (Melissianos *et al*. 2022). To the authors best knowledge, the international literature currently lacks a detailed presentation of the steps that need to be taken for deriving analytical seismic fragility curves for building-type structures supporting critical equipment in oil refineries.

In order to accomplish the set goals, the paper is organised as follows: Initially, a number of typical to an oil refinery equipment-supporting structures were selected and consequently presented along with the characteristics of the supported industrial machinery. In the next section, the developed structural models are described and the assumptions made are justified. Subsequently, the damage states for the considered industrial open-frame building typologies and the associated failure modes are presented. Next, the computation of seismic demands and the adopted analytical fragility assessment framework are discussed. Finally, the results of the study are summarised and the most important findings and main conclusions are outlined.

2 CASE STUDIES

Three reinforced concrete moment-resisting frames, namely RC1, RC2 and RC3, and two steel-braced frames, namely ST1 and ST2, were analysed. Illustrations of these structures are shown in Figure 1 and the geometry along with the respective dynamic properties are reported in Table 1. The considered structural typologies and equipment are typical of refineries, where numerous different processes, such as crude oil distillation, vacuum distillation, diesel hydro-treating, fluid catalytic cracking, sulphur recovery, and isomerisation take place to transform crude oil into useful products, namely gasoline, jet diesel, marine oil, liquefied petroleum gas, asphalt, etc. (Fahim *et al*. 2010).

The design of the pertinent structural members for those high importance structures aims, among others, to minimise lateral deformations due to external stressors (e.g., earthquakes), as well as to prevent damage on the nested equipment and/or piping that would disrupt the production process across the facility. Moreover, the flammable substances that go through the equipment as well as any plans for future expansion, impose stricter fire-safety criteria and loading conditions versus other high-importance buildings. Such a design procedure typically results in structural members of increased cross-sections, which in turn leads to overdesigned structures. The assets considered herein were designed assuming a European site of moderate seismicity. Yet, due to their significant overstrength, little (if any) structural damage is anticipated even during strong ground shaking, under the assumption that appropriate routine maintenance is exercised throughout the lifetime of the structures.

The same does not necessarily hold true for non-structural damage. Structural overdesign leads to high stiffness and, in turn, to high floor acceleration demands that increase with elevation. There is also higher chance for the periods of the (often stiff) nested equipment falling close to one of the predominant vibration modes of the supporting structure. Then, the already high acceleration demands can be amplified by several orders of magnitude (Kazantzi *et al*. 2020), potentially leading to equipment damage with uncontrolled leakage or fire, endangering the entire structure-equipment system or even the entire plant (e.g., Gillman and Le May 2007;

Khan and Amyotte 2007). In fact, as will be showcased later on, such damages govern the overall seismic performance of the structure-equipment system.

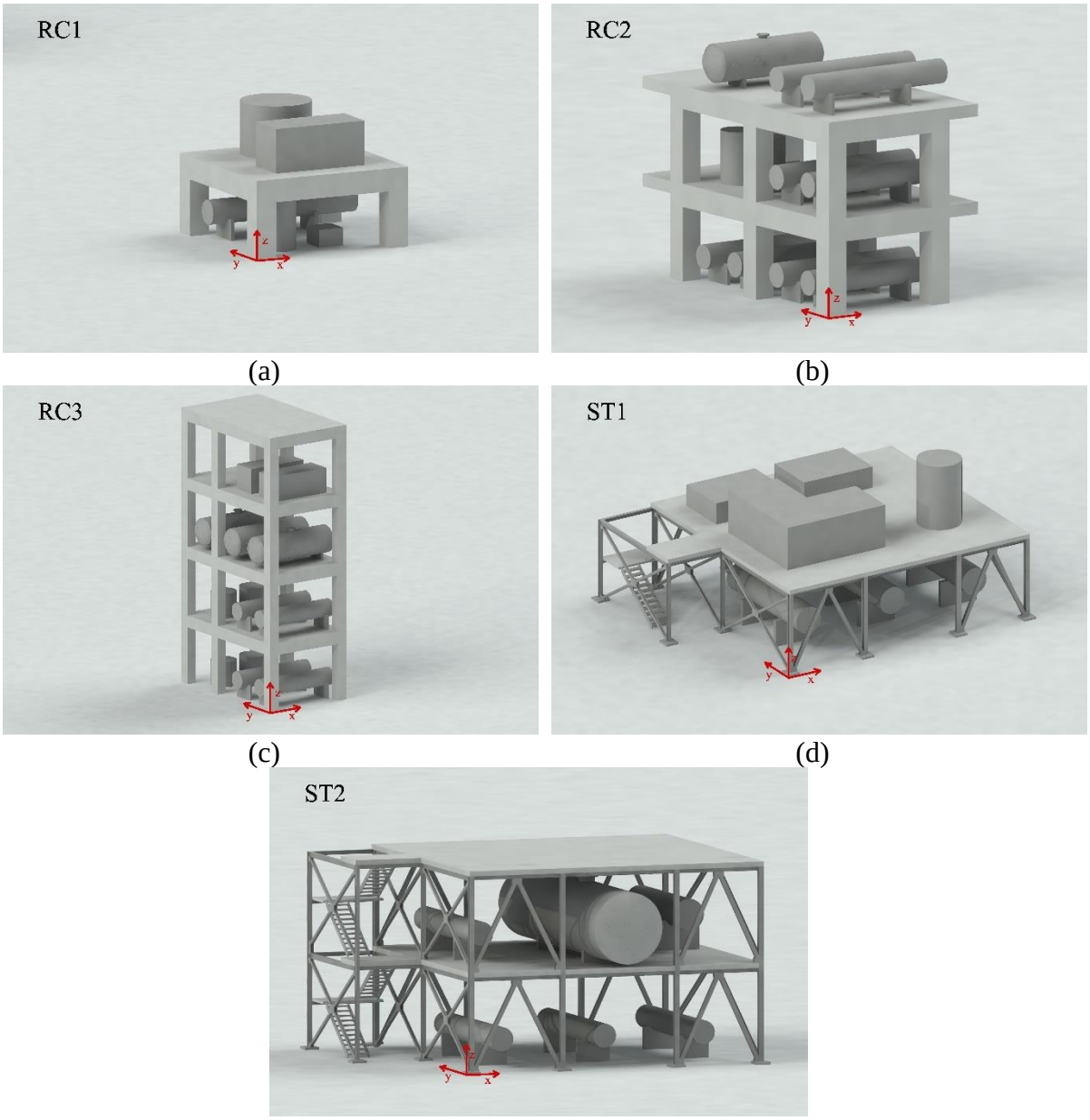

Figure 1. 3D representation of the (a) 1-storey RC (RC1), (b) 2-storey RC (RC2), (c) 4-storey RC (RC3), (d) 1-storey braced steel (ST1), and (e) 2-storey braced steel (ST2) buildings along with their nested process equipment.

Table 1: Geometry and dynamic properties of the case study buildings.

Building ID	No of storeys	Storey height (m)	Floor plan x · y (m^2) *	Fundamental period T_x(sec)	Fundamental period T_y(sec)	Total mass** (kg)
RC1	1	4.50	9.40 · 9.40	0.08	0.08	173752
RC2	2	5.50	8.20 · 15.20	0.21	0.20	612989
RC3	4	5.50	7.30 · 11.80	0.57	0.54	596924
ST1	1	4.00	12.07 · 11.40	0.10	0.07	45952
ST2	2	4.00	12.07 · 11.40	0.16	0.10	89806

*Excluding the area of stairs and cantilevers

**Including the nested equipment other than that of the ground level

Table 2: Nested equipment items per case study building with global axis designations per Figure 1.

Building ID	Elevation (mm)	Item	Mass (kg)	Vibration period range T_x(sec)	Vibration period range T_y(sec)	OS x	OS y	IC*
RC1	±0,000	Pump	500	0.10	0.10	1.10	1.10	II
		Vessel	2,500	0.10 – 0.20	0.10 – 0.20	1.20	1.20	I
		Heat exchanger	10,000	0.30 – 0.50	0.10 – 0.20	1.20	1.50	III
	+4,500	Vessel	10,000	0.10 – 0.20	0.10 – 0.20	1.20	1.20	I
		Vacuum charge	10,000	0.10 – 0.20	0.10 – 0.20	1.50	1.50	II
RC2	±0,000	4 × Heat exchanger	10,000	0.30 – 0.50	0.10 – 0.20	1.20	1.50	III
	+5,500	2 × Heat exchanger	10,000	0.30 – 0.50	0.10 – 0.20	1.20	1.50	III
		2 × Vessel	2,500	0.10 – 0.20	0.10 – 0.20	1.20	1.20	I
		2 × Pump	500	0.10	0.10	1.10	1.10	II
	+11,000	2 × Heat exchanger	4,000	0.30 – 0.50	0.10 – 0.20	1.20	1.50	III
		Horiz. vessel	7,500	0.30 – 0.50	0.10 – 0.20	1.20	1.50	II
RC3	±0,000	2 × Heat exchanger	5,000	0.30 – 0.50	0.10 – 0.20	1.20	1.50	III
		2 × Vessel	1,500	0.10 – 0.20	0.10 – 0.20	1.20	1.20	I
	+5,500	2 × Heat exchanger	5,000	0.30 – 0.50	0.10 – 0.20	1.20	1.50	III
		2 × Vessel	1,500	0.10 – 0.20	0.10 – 0.20	1.20	1.20	I
	+11,000	3 × Horiz. vessel	7,500	0.30 – 0.50	0.10 – 0.20	1.20	1.50	II
	+16,500	2 × Reactor	2,000	0.10 – 0.20	0.10 – 0.20	1.50	1.50	III
ST1	±0,000	3 × Exchanger	2,500	0.10 – 0.20	0.30 – 0.50	1.50	1.20	III
	+4,000	2 × Reactor	2,000	0.10 – 0.20	0.10 – 0.20	1.50	1.50	III
		Electrical equipment	4,500	0.10 – 0.20	0.10 – 0.20	1.20	1.20	I
		Vessel	500	0.10 – 0.20	0.10–0.20	1.20	1.20	I
ST2	±0,000	3 × Converter	5,000	0.10 – 0.20	0.30 – 0.50	1.50	1.20	III
	+4,000	Converter	5,000	0.10 – 0.20	0.30 – 0.50	1.50	1.20	III
		Horiz. vessel	7,000	0.10 – 0.20	0.30 – 0.50	1.50	1.20	II
		Exchanger	2,500	0.10 – 0.20	0.30 – 0.50	1.50	1.20	III

* Importance Categories (IC) according to Table 3

Table 3: Process equipment Importance Categories (IC).

IC	Importance	Impact on refining process
I	Low	Failure associated with marginally no disruption
II	Medium	Failure associated with limited disruption
III	High	Failure associated with severe disruption

Table 2 summarises the properties, the locations along the building height and the assumed Importance Classes (ICs) for the industrial machineries that were assumed to be nested in each one of the considered buildings. Each equipment was paired to an IC as per Table 3, in an attempt to capture whether, and to what extent, a potential failure is linked to disruptions of the overall refining process. To that effect, the assignment of the considered equipment to ICs was mostly based on expert opinion and it is restricted in the realm of oil refinery plants, since the consideration of other kind of industrial plants (e.g., chemical) could lead to substantially different disruption consequences even for the same or similar type of equipment. Yet, even in the case of oil refinery plants, different IC assumptions could be made by other experts for the same type of equipment based on its function within the plant.

3 REDUCED-ORDER MODELLING

Reduced-order building models were utilised, in an attempt to balance the accuracy and the computational efficiency needed in practical analytical fragility applications. Given the high-strength low-ductility design, which is anticipated to restrict the structural response to the elasticity realm even for the highest intensity levels that will be considered in the fragility

assessment, all buildings were modelled in 3D using elastic beam-column elements of the OpenSees platform (McKenna and Fenves 2001). A rigid diaphragm was assigned at each floor level, essentially implying that the floor slabs are thick enough to provide sufficient in-plane rigidity. Rayleigh damping was employed, assigning damping ratios of 5% and 2% for the reinforced concrete and the steel buildings, respectively, to the first and second global translational modes of vibration.

The non-structural components (i.e., equipment items) were not explicitly modelled. Instead, they were introduced to the building models as point masses only. Disregarding the dynamic interaction between the primary structure and the non-structural components is a modelling approach that has been adopted in the past for building structures in industrial facilities (e.g., Butenweg and Holtschoppen 2013). Strictly speaking, this assumption is valid when the mass of the components is approximately less than 1% of the building mass (Taghavi and Miranda 2008), a condition that is often violated herein, especially in the case of the lightweight, yet stiff, steel buildings. ASCE 7-16 (ASCE/SEI 2017) offers a less restrictive rule requiring explicit modelling of non-structural components whose weight exceeds 25% of the effective seismic weight of the supporting structure. Nevertheless, the impact of disregarding component-structure interaction on the estimated fragilities cannot be fully determined a priori, heavily depending on the case at hand. For instance, a recent shake table testing campaign of a full-scale three-storey steel moment-resisting frame, revealed that the relative displacements between the primary structure and the non-structural components could result in increased stresses (Butenweg *et al.* 2020; 2021). On the other hand, Merino Vela *et al*. (2019) investigated a single steel braced frame-tank system considering both coupled and uncoupled models, concluding that tank-structure interaction only marginally affected the fragility estimates for the structure or the components. For the cases at hand, the results of Taghavi and Miranda (2008) suggest that the combination of overdesigned stiff structures with fairly rigid non-structural components will result to moderately conservative fragilities when ignoring dynamic interaction. Nevertheless, this is certainly an issue that merits further investigation, yet it is beyond of the scope of this study.

Based on the preceding discussion, Peak Floor Acceleration (PFA) demands were recorded at the anchor points of non-structural components that are located on floor levels other than the ground; these were consequently converted to Peak Component Acceleration (PCA) demands utilising the simplified equations for evaluating the component acceleration amplifications factor, a_p, proposed by Kazantzi *et al.* (2020). This factor essentially quantifies the ratio of elastic PCA over the PFA, while accounting for component damping and the non-trivial amplification of demands when the fundamental period of the non-structural component is close to a predominant modal period of the supporting structure. For components located at the ground level, the component acceleration demands are represented by the pertinent ground spectral acceleration ordinates evaluated at the component periods. In all cases, a component damping ratio of 2% was adopted. This is a highly uncertain parameter, as has been demonstrated before by several experimental studies (e.g. Watkins *et al.* 2009; Astroza *et al.* 2015). Still, the choice of 2% was considered to be a characteristic value for the non-structural components of interest, if not somewhat conservative.

4 DAMAGE STATES AND FAILURE MODES

The definition of Damage States (DS) for the considered industrial building typologies requires identifying the most likely failure modes, while also sorting them out in terms of their impact on the integrity of the structural system in question. Contrary to modern loss assessment frameworks, exemplified by FEMA P-58 (2018), the focus is not on aggregating losses component by component, but rather on identifying the most critical one that will trigger cascading failures (e.g., Girgin *et al.* 2019). Thus, while we do consider individual components,

they are only employed to inform fragility at the global building level. Table 4 summarises the four distinct global DSs along with their associated failure modes that were considered by identifying the damage in the drift-sensitive (structural/non-structural), and acceleration-sensitive (non-structural) components.

4.1 Drift-sensitive structural and non-structural components

The four identified DSs were paired with specific maximum (over time and elevation) Interstorey Drift Ratio (IDR) Limit-State (LS) thresholds for characterising the damage induced in structural elements and in drift-sensitive non-structural components attached to the building, such as piping. IDR is deemed to be the most suitable Engineering Demand Parameter (EDP) for this purpose. Some guidance can be found in HAZUS-MH (FEMA 2003) where IDR values of 0.5%, 1%, 3% and 8% are quoted for attaining Slight to Complete structural damage of high-code low-rise steel and RC buildings. These values drop down to 0.5%, 0.8%, 2% and 5%, respectively, for low-code designs. For drift-sensitive non-structural damage, the values of 0.4%, 0.8%, 2.5% and 5% are used for all code levels. Our structures fall somewhere between the two, having high strength (i.e., high code) but typically low-to-moderate ductility (low code). Thus, the early damage state of DS1 is closer to the high-code standard, while post-yield DS2 and DS3 would better conform to the low-code one. Herein, DS1 is attained at IDR of 1%, as specified by EN1998-1 (CEN 2004) for buildings without partition walls. For moderate damage DS2, a threshold of 2% was chosen to consider, among others, any damage that is likely to occur in the vertical piping spanning across different storeys. The near-collapse DS3 is associated with a 4% IDR threshold (Table 4). While much discussion can be had on the particulars of these choices, it is of little consequence as drift-based fragilities do not govern the overall performance. It should be pointed out that differential displacements between adjacent machinery located at the same floor level, that are likely to induce damages to the connecting piping system (especially in the case of unanchored machinery that is likely to undergo sliding or rocking) and consequently to the supporting structure are not taken into account. Yet, for anchored equipment, like those considered in this study, our decision to disregard this failure mode is expected to have minor impact on the overall seismic performance, since anchorage failure, which was explicitly accounted for, will precede. Having said that, the issue of differential deformation of neighbouring structures connected by piping can be more critical, but it is not covered herein as only single buildings are considered.

Table 4: Building DS classification and associated LS definitions due to damage on structural and non-structural components.

DS	LS threshold	
	Drift-sensitive structural and non-structural components	**Acceleration-sensitive non-structural components**
DS0	—	—
DS1	$IDR > 1\%$	Anchorage failure of at least one component of IC I
DS2	$IDR > 2\%$	Anchorage failure of at least one component of IC II
DS3	$IDR > 4\%$	Anchorage failure of at least one component of IC III

4.2 Acceleration-sensitive non-structural components

The same four DSs were also defined in terms of damage in the nested acceleration-sensitive non-structural components (Table 2). In this case, the DSs were associated with damage that is likely to occur primarily in the component anchorage system, assuming that the component itself does not fail earlier. The first failure of an IC I/II/III component, determined by the

exceedance of its anchorage capacity, signifies the attainment of DS1/DS2/DS3, respectively, as per Table 4.

In absence of detailed data regarding the actual configuration and hence capacity of the equipment anchorage systems, they were assumed to be designed per the recommendations of EN1998-1 as non-dissipative elements, with the added overstrength prescribed in Table 2 due to typical overdesign in practice. To this end, initially, EN1998-1 Annex 4.3.5 "Non-structural elements" (CEN 2004) was utilised to evaluate the design seismic coefficient, S_{ac}, for each component:

$$S_{ac} = a \cdot S \cdot \left[\frac{3 \cdot \left(1 + \frac{z}{H}\right)}{1 + (1 - T_a/T_1)^2} - 0.5 \right] \geq a \cdot S \quad (1)$$

In Eq. (1), a is the ratio of the design ground acceleration on type A ground over the acceleration of gravity, taken as 0.24 for the site of interest (typical of moderate-to-high seismicity); S is the soil factor, equal to 1.20 for the assumed soil type B; T_a is the fundamental period of vibration of the non-structural component in the direction of interest, taken as the median value of the pertinent period ranges reported in Table 2; T_1 is the fundamental vibration period of the building in the direction of interest ($T_{1\mathrm{x}}$ or $T_{1\mathrm{y}}$); z is the elevation of the supporting floor relative to the ground; H is the building height.

In design practice, for buildings of low/moderate height, equipment anchorage is often designed under the assumption that it resides on the top of the building, essentially resulting in $z/H = 1$, regardless of elevation. This is done in the interest of construction standardisation, and it is deemed to be a reasonable assumption given the minor contribution of the anchors in the overall building cost. It should be also noted that both the period ranges of the ancillary components reported in Table 2 and the adopted median period T_a are highly uncertain parameters and were only provided as best estimates for the considered non-structural components. In cases where such information is not provided by the component manufacturer or any other credible source of information, it is preferable to design the components assuming they are tuned to the period of the supporting structure. The latter, along with the assumption regarding the location of the component (i.e., top of the building), form a condition that yields the highest seismic design coefficient S_{ac} according to Eq. (1).

Then, the final component capacity spectral acceleration $S_{a_{cap}}$ for each one of the two orthogonal directions (x and y) is calculated as:

$$S_{a_{cap}} = \frac{S_{ac} \cdot \gamma_a}{q_a} \cdot OS \cdot \mathrm{g} \quad (2)$$

In Eq. (2), S_{ac} is the seismic coefficient of Eq. (1); γ_a is the component importance factor, assumed equal to 1.50 as proposed by EN1998-1 for tanks and vessels containing toxic or explosive substances; q_a is the behaviour factor of the component, taken equal to 1.00, essentially denoting an elastic design for the anchorage; OS is an overstrength factor, based on engineering judgement (see Table 2); g is the gravity acceleration.

It should be noted that the assumed *OS* factors were determined accounting for the anchorage system of each equipment and its IC. For instance, the anchorage in the case of large compact equipment (e.g., vacuum charge) was considered to be overdesigned with an *OS* equal to 1.50 in both directions, while for smaller compact equipment, such as the pumps, a lower *OS* factor equal to 1.10 was assumed. For vessels at IC I, an *OS* factor equal to 1.20 was considered in both directions, while for horizontal vessels at IC II, as well as for heat exchangers and exchangers at IC III the *OS* factor was assumed equal to 1.20 in the relatively more flexible (local) longitudinal direction of their anchorage system (in view of the higher local deformations) and equal to 1.50 in the stiffer (local) transverse direction.

The component capacity acceleration $S_{a_{cap}}$ was then compared to the demand acceleration $S_{a_{dem}}$ that was obtained for the above-ground supported components by amplifying the PFA computed at the anchorage points (via response-history analysis of the 3D building models) with the component amplification factor a_p of Kazantzi *et al.* (2020) to account for component dynamic characteristics:

$$S_{a_{dem}} = PFA \cdot a_p \tag{3}$$

5 SEISMIC DEMAND

5.1 Intensity Measures, site hazard and ground motions

There are several metrics available in the literature to be considered as Intensity Measures (IM), spanning across asset-aware (e.g. first-mode spectral acceleration), or asset-agnostic (e.g. peak ground acceleration or velocity) scalar or vector choices. Adopting an asset aware IM, such as the first-mode spectral acceleration, would offer excellent results for any specific structure, especially given the elastic models adopted. Still, this would come at the cost of having a different IM for each structure. Targeting a refinery-wide application (see Melissianos *et al*. 2022), the fragility curves were instead assessed for the asset-agnostic peak ground acceleration, PGA, a reference IM often used in fragility studies, and for the spectral acceleration averaged over a period range, $AvgS_a$ (e.g., Cordova *et al*. 2000; Vamvatsikos and Cornell 2005; Tsantaki *et al.* 2017; Eads *et al*. 2015). The latter has been shown to be a fairly efficient and sufficient IM for building non-structural components (Kazantzi and Vamvatsikos 2015) as well as for liquid storage tanks (Bakalis *et al.* 2018), while its hazard is readily computable (Cordova *et al*. 2000). Both IMs were evaluated in the geomean, rather than the arbitrary component sense, to comply with the majority of existing ground motion prediction equations. For *PGA*, this entails taking the geometric mean of the respective values recorded in the two horizontal directions. For $AvgS_a$, we employed geomean spectral acceleration ordinates for periods spanning 0.1sec to 1sec at 0.1sec intervals.

A set of 30 "ordinary" (i.e., non-pulse-like, non-long-duration) natural ground motion records was employed to carry out the response-history analyses. It should be noted that the number of the records employed for the evaluation of the imposed seismic demands is deemed to be sufficient (e.g., Baltzopoulos *et al*. 2019) and beyond what it is prescribed even in the most current seismic assessment methodologies. For instance, FEMA P-58 (2018) recommends 7 to 11 (or more) pairs of ground motion records depending on whether the records match well or not the shape of the targeted spectrum over the period range of interest. The records used herein were selected by Bakalis *et al*. (2018) for the same definition of $AvgS_a$, using the conditional spectrum approach (Lin *et al*. 2013; Kohrangi *et al*. 2017) to achieve hazard consistency with the considered site. Given the short period structures that were considered in the study of Bakalis *et al*. (2018), the selection of records was deemed to be appropriate also for the case at hand and for both IMs employed, as hazard consistency is not sensitive to mild period and intensity changes (Lin *et al*. 2013; Kohrangi *et al*. 2020).

5.2 Response assessment via IDA

The selected ground motion set was employed in Incremental Dynamic Analysis (IDA, Vamvatsikos and Cornell 2002) using ten IM levels to assess the performance of each structure. Per Section 4, IDR (maximum over all stories) was adopted for monitoring the integrity of the drift-sensitive components, and PFA (at individual stories) for acceleration-sensitive ones. A set of IDA curves is indicatively presented in Figure 2 for the 2-storey reinforced concrete building (RC2 in Figure 1) to obtain an understanding of the response. The fractile (16/50/84%) IDA curves are shown for $AvgS_a$ and the two selected EDPs. Evidently, the IDA curves are straight lines because the models are elastic.

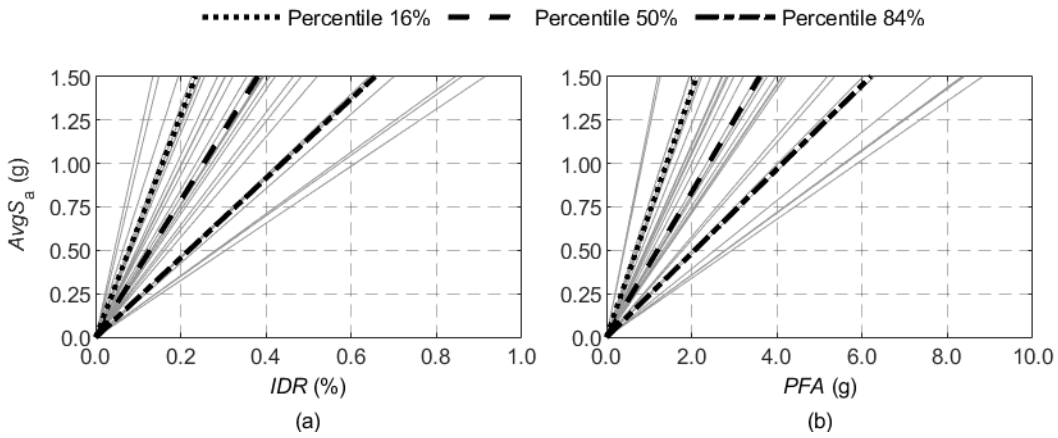

Figure 2. Single record and 16/50/84% fractile IDA curves for RC2; (a) maximum IDR versus (b) maximum PFA.

6 SEISMIC FRAGILITY ASSESSMENT

6.1 Fragility definition

Once the demand and capacity of the considered structures and their nested equipment have been determined, one may proceed to the fragility evaluation. In principle, fragility curves constitute a key element in a seismic risk assessment and are used for quantifying the damage potential of the assets of interest. Thus, the probability of exceeding a specific LS, or equivalently the probability of being in a particular DS, is computed. The derivation of analytical fragility curves via response-history analyses has been demonstrated in several past studies (e.g., Dymiotis *et al.* 1999; Kwon and Elnashai 2006; Kazantzi *et al.* 2011; Bakalis and Vamvatsikos 2018). The fragility is essentially a function of the IM and may be expressed as

$$F_{LS}(IM) = P[D > C_{LS}|IM] \tag{4}$$

where D is the EDP demand, and C_{LS} is the EDP capacity threshold paired to a specific LS. Under a typical lognormality assumption (Cornell *et al*. 2002), fragility may be expressed as:

$$P[D > C_{LS}|IM] = P[LS \text{ violated} \mid IM] = \Phi\left(\frac{\ln IM - \ln IM_{LS50}}{\beta_{LS}}\right) \tag{5}$$

where IM_{LS50} is the median IM value required to violate a given EDP threshold per Table 4, and β_{LS} is the dispersion, equal to the standard deviation of the natural logarithm of the data.

6.2 Combined component approach

Drift-sensitive fragilities were treated in a global sense, via the maximum IDR over all floors. Given that acceleration-sensitive components govern response, they received a component-specific treatment, accounting for demand and capacity on a component-by-component basis and necessitating a distinction between two flavours of fragility curves. While an "individual" component fragility curve refers to the probability of exceeding the capacity of a specific (acceleration-sensitive) component given the IM, a "combined" component fragility curve denotes the probability of exceeding the capacity of *any component within a specific IC in the building* (see Table 2). According to the DS definition in Table 4, this condition essentially signals the transition of the entire asset to a specific DS due to non-structural damage in the acceleration-sensitive equipment (see Figure 3). The following algorithm summarises the procedure to derive "combined" component fragility curves.

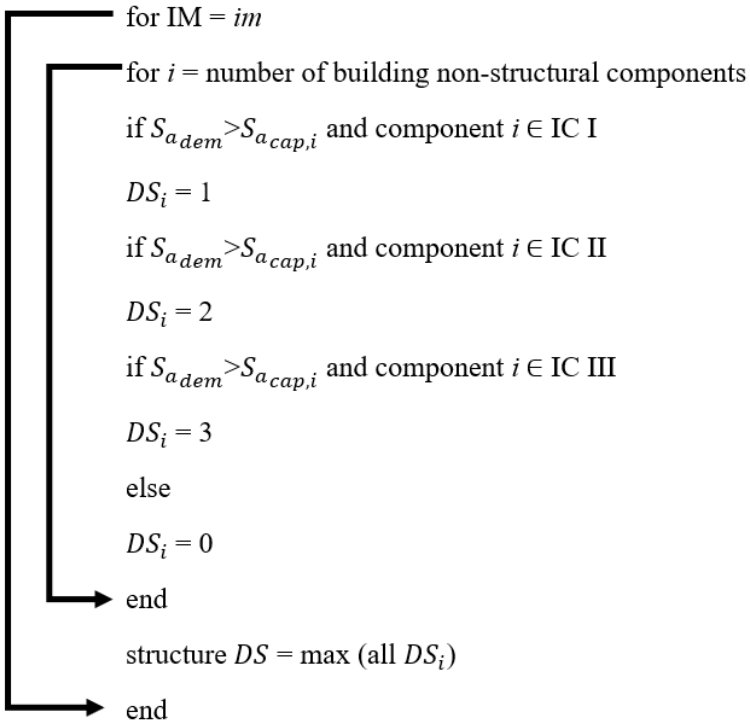

Figure 3. Pseudo-algorithm outlining the process of deriving the "combined" component fragility curves.

It should also be noted that the parameters of the combined fragility curves (i.e., median and dispersion) for a particular building asset do not necessarily coincide with those of the most vulnerable component from each IC, with the combined component fragilities being in the majority of the cases the more adverse ones. This outcome stems from the correlation of demands across different floors, as well as the existence of multiple equipment items of similar (or the same) capacity within each building. Simply accounting for the worst component can be grossly inaccurate. Alternatively, one could employ simplified combination rules (Pulkkinen 1993) to assess the combined fragility for what is essentially a multicomponent series system (Melchers and Beck 2017), capturing at least some of the interaction among the individual fragilities. In the present study, we opted for a full combination, tracking in detail the failure probability of individual components during each response history analysis, aggregating the results per IC category at each IM level, and forming the exact combined fragilities. In all cases, pertinent uncertainties were fully accounted for, as described in the following section.

6.3 Uncertainty propagation

Both aleatory and epistemic uncertainties were considered. For a well-constructed and carefully maintained structure, the former is dominant, as demonstrated in several past studies (e.g., Kwon and Elnashai 2006; Kazantzi *et al.* 2008; Kazantzi *et al.* 2014). Herein, the randomness associated with the seismic input (record-to-record variability) was accounted via utilising a suite of 30 ground motion records as per Section 5.1. Further to the above, with reference only to the above-ground acceleration-sensitive non-structural components, the component amplification factor a_p, was also assumed to be lognormally distributed with a median per Kazantzi *et al*. (2020) and a dispersion equal to 0.30. The latter may be considered a demand-related uncertainty source that attempts to capture the a_p-demand variability per record, since its median was obtained on the basis of floor accelerations recorded on different buildings from those considered in this study, different floor levels, and acceleration sensors that were installed

at different floor plan locations. The component acceleration capacity $S_{a_{cap}}$ was assumed to be normally distributed, having a median value equal to that obtained from Eq. (2) and a coefficient of variation (CoV) equal to 0.20 (see also FEMA 2018).

For each acceleration-sensitive component nested in a particular building, $N = 100$ component acceleration demand realisations were randomly generated per record (Figure 4), using the aforementioned a_p distribution to account for the intra-record demand uncertainties ($S_{a_{dem}}$ via sampling 100 a_p values). For simplicity, per each individual record a single set of 100 a_p realisations was utilised across all intensity levels. Similarly, 100 realisations of component acceleration capacity ($S_{a_{cap}}$) were generated for each component type (e.g., for all heat exchangers nested in a particular building); essentially, a perfect correlation of capacities was assumed among items of the same type, but zero correlation among different types. The demand realisations were randomly paired with the capacity realisations, to account for zero demand–capacity correlation. Hence, for each individual record, for the i^{th} demand–capacity pair out of the N produced ($i \in [1, N]$), and the j^{th} ground motion record intensity level increment ($j \in [1,10]$), failure is signalled by

$$S_{a_{dem}}(i,j) \geq S_{a_{cap}}(i) \Leftrightarrow a_p(i) \cdot PFA(j) \geq S_{a_{cap}}(i) \quad (6)$$

A summary of the uncertainties considered in this study is also provided in Table 5.

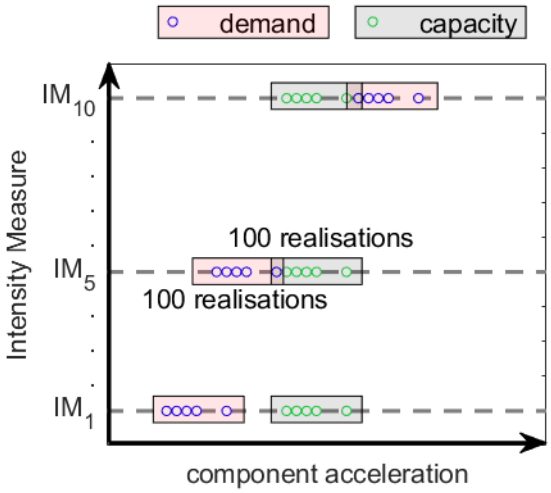

Figure 4. Intra-record demand–capacity uncertainty propagation for a single non-structural acceleration-sensitive component and one record: At each of 10 IM levels, 100 realisations of component acceleration demand are generated and randomly paired with 100 capacity realisations generated per component type. Where demand and capacity overlap, component failure is signified.

The impact of the intra-record uncertainty in demand $S_{a_{dem}}$ and capacity $S_{a_{cap}}$ is further explored by considering three distinct cases for the components of the RC2 building. The combined acceleration-sensitive component fragilities for DS3 were computed for three cases: Case 1 accounts for both a_p (demand) and capacity uncertainty (full probabilistic approach), Case 2 accounts only for a_p uncertainty (partial probabilistic approach), and Case 3 disregards the uncertainty in both a_p and capacity (so called "deterministic", although record-to-record variability is still incorporated). According to Figure 5, the impact of the probabilistic characterisation of capacity is minimal due to its negligible effect on the median and the dispersion of the combined fragility when full (Case 1) and partial (Case 2) approaches are compared. This comes as no surprise, given the dominant record-to-record variability (included in all cases), plus the 0.3 dispersion (akin to a CoV for lognormal variables) of the demand, compared to only 0.2 for the capacity. The impact of capacity uncertainty would become more

significant in cases of higher dispersion, as in the case of low construction quality or deficient maintenance practices (Kazantzi *et al*. 2014), which are not expected in refineries. Comparing the full probabilistic (Case 1) with the "deterministic" (Case 3), one can observe notable differences at least on the median; the fragility dispersion is still dominated by the record-to-record variability due to the less-than-optimal choice of asset-agnostic IMs. Therefore the a_p uncertainty is worth considering despite the additional computational cost. In the subsequent sections, only the findings of the full probabilistic approach are presented. For the sake of completeness, a lognormal distribution with 0.20 dispersion is also applied to the IDR capacity limits for drift-sensitive components, yet again with little actual effect.

Table 5: Uncertainty propagation in the seismic fragility assessment.

Components	**Uncertainties**	
	Demand	**Capacity**
Structural and drift-sensitive non-structural	Record-to-record variability	IDR limit: lognormally distributed with median per Table 4 and dispersion of 0.20
Acceleration-sensitive non-structural	• Intra-record: Component amplification factor a_p: lognormally distributed with median per Kazantzi *et al*. (2020) and dispersion of 0.30 • Record-to-record variability	Component acceleration capacity $S_{a_{cap}}$: normally distributed with median per Eq. (2) and CoV of 0.20

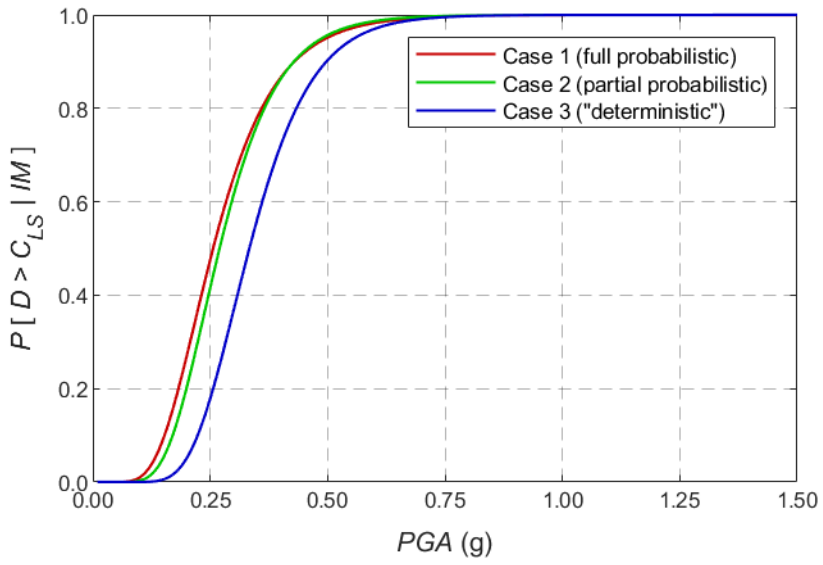

Figure 5. Combined component fragility curves for DS3 considering alternative uncertainty characterisation: Case 1 (full probabilistic): median $PGA = 0.26$g, Case 2 (partial probabilistic): median $PGA = 0.27$g, and Case 3 ("deterministic"): median $PGA = 0.33$g. Results refer to the RC2 building.

7 RESULTS AND DISCUSSION

7.1 Drift-sensitive structural and non-structural fragilities

A drift-sensitive component fragility depicts the probability of a building violating a specific *IDR* limit (see Table 4) that is likely to induce damages in its structural components or in drift sensitive non-structural ones. Their median and dispersion are summarised in Table 6 for all

five buildings, three DSs, and IMs considered. As expected for well-designed, constructed, and maintained building-type refinery structures, the medians in most cases are in excess of 2g. In other words, they are inconsequential for the overall asset performance.

On another note, the dispersion of the structural fragility was overall found to be higher when computed for $AvgS_a$ compared to PGA, except for the case of the 4-storey RC building (RC3). This can be attributed to the periods of 0.1 – 1.0sec assumed for $AvgS_a$, whereas the fundamental periods are within the 0.1 – 0.6sec range (Table 1). This would have been reasonable for structures that are expected to go inelastic, but not so for elastic ones. However, our intention was to assume a range of periods that is representative for a variety of assets that could be found in a refinery, since risk assessment is typically done in a plant-wide sense. Nevertheless, if this is not the case, then a more representative range of periods for $AvgS_a$, or even a single spectral acceleration ordinate at about 0.2 to 0.4sec would be a better choice, resulting in reduced dispersion estimates.

Table 6: Median and dispersion of drift-sensitive component fragilities

Damage States	PGA		$AvgS_a$	
	median (g)	dispersion	median (g)	dispersion
	1-storey RC (RC1)			
DS1 – 3	> 2.00	0.28 – 0.30	> 2.00	0.53 – 0.56
	2-storey RC (RC2)			
DS1 – 3	> 2.00	0.35	> 2.00	0.49 – 0.54
	4-storey RC (RC3)			
DS1	0.90	0.55	1.26	0.31
DS2	1.79	0.55	> 2.00	0.31
DS3	> 2.00	0.55	> 2.00	0.31
	1-storey steel (ST1)			
DS1 – 3	> 2.00	0.45	> 2.00	0.58
	2-storey steel (ST2)			
DS1 – 3	> 2.00	0.45	> 2.00	0.59 – 0.61

7.2 Combined acceleration-sensitive component fragilities

The combined acceleration-sensitive component fragility curves are evaluated for the considered assets. To provide a comparative sense of component damageability, indicative fragilities are also presented for the individual components. Two characteristic examples of RC2 and ST2 are subsequently examined.

The individual fragility curves of the 13 components (see Table 2) nested in the 2-storey RC building (RC2) are depicted in Figure 6(a, b) for PGA and $AvgS_a$, respectively, computed separately for each one of the principal (x, y) axes to account for the different dynamic characteristics of building and equipment. There are four components at the ground level belonging to IC III, six at the 1st floor belonging to all three ICs, and another three at the roof level belonging to IC II and III. The weakest (most critical) components for IC I are the first-floor vessels in the x-direction (see Figure 1b), for IC II the roof-level horizontal vessel in the y-direction, and for IC III a roof-level heat exchanger in the y-direction.

The median and the dispersion of the weakest component fragilities presented in Figure 6 are also summarised in Table 7. Interestingly, it was found that the failure of the weakest component belonging to IC III occurs prior to failure of the other components belonging to ICs that are paired with less severe DSs. Hence, for the RC2 asset, DS3 will be the most critical,

not only because its attainment denotes more severe damageable consequences for the building but also because it occurs at lower IM levels compared to the less severe DSs. This observation is by no means unusual and it also holds for other buildings. From a practical point of view, to improve the seismic performance of such assets, one may consider strengthening the anchorage of the critical IC III components or consider repositioning (if possible) such vulnerable components, e.g. move the critical heat exchangers located at the roof level for RC2 to lower levels to reduce the imposed acceleration demands.

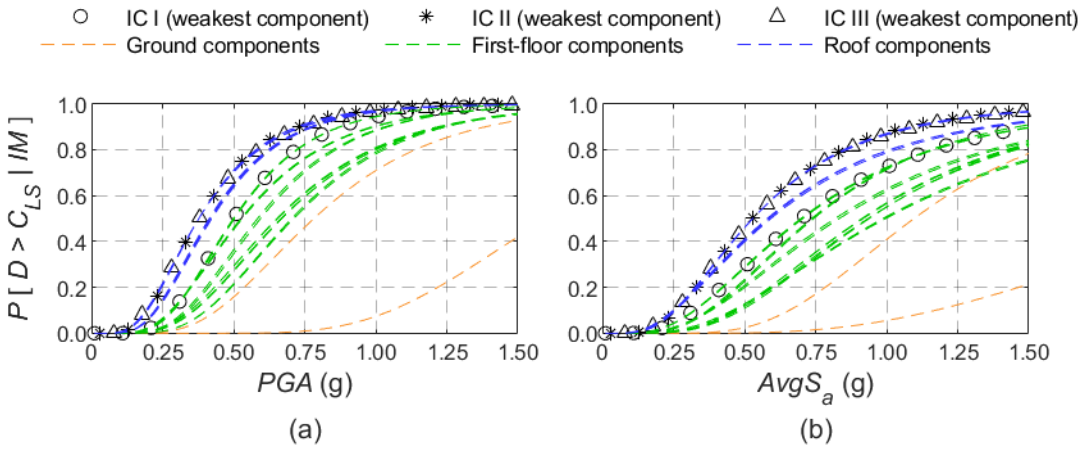

Figure 6. Individual component fragility curves for the RC2 building non-structural acceleration-sensitive components using as an IM (a) PGA and (b) $AvgS_a$. The critical component for each IC is shown with markers; the resulting fragilities for ICs II (star) and III (triangle) almost coincide.

Table 7: Median and dispersion of the individual component fragilities for the critical component of each IC (RC2 building).

Weakest component per IC	PGA		$AvgS_a$	
	median (g)	**dispersion**	**median (g)**	**dispersion**
IC I: First-floor vessel (x direction)	0.50	0.44	0.70	0.60
IC II: Roof horizontal vessel (y direction)	0.38	0.51	0.53	0.56
IC III: Roof heat exchanger (y direction)	0.38	0.53	0.53	0.58

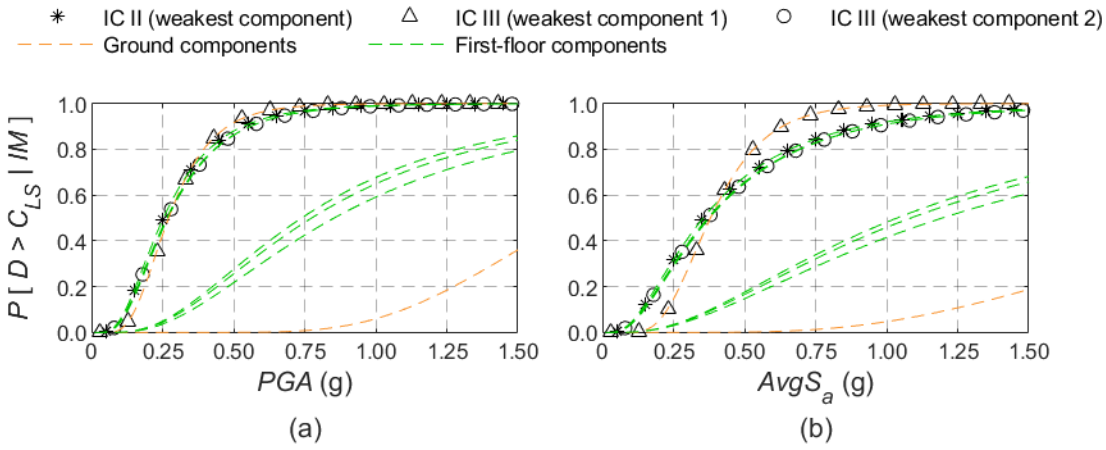

Figure 7. Individual component fragility curves for the ST2 building non-structural acceleration-sensitive components using as an IM (a) PGA and (b) $AvgS_a$. The critical component for each IC is shown with markers; there are two candidate worst cases for IC III in both figures as their fragilities intersect.

Table 8: Median and dispersion of the individual component fragilities for the critical component of each IC (ST2 building). There are two candidate worst cases for IC III, none for IC I.

Weakest component per IC	PGA		$AvgS_a$	
	median (g)	dispersion	median (g)	dispersion
IC I: No component exists	–	–	–	–
IC II: First-floor horiz. vessel (x direction)	0.25	0.58	0.35	0.74
IC III: Ground converters (y direction)	0.27	0.44	0.38	0.40
IC III: First-floor exchanger (x direction)	0.26	0.58	0.37	0.74

The individual fragility curves of the equipment supported by the 2-storey braced steel building (ST2) are shown in Figure 7(a,b) for PGA and $AvgS_a$, respectively. Once again, the fragilities illustrated in Figure 7 and summarised in Table 8 correspond to all six equipment items in ST2, with separate fragilities evaluated for each one of the components' dominant axes (see Table 2). In this case almost all components belong to the IC III, with the only exception being the horizontal vessel located at the first floor that belongs to IC II. Hence, the weakest component for IC II is this first-floor horizontal vessel, along the global x direction (see Figure 1e). By contrast, as can be inferred from the fragilities presented in Figure 7, there are two candidate individual fragilities to characterise the critical component belonging to IC III. They are associated with the ground-floor converters along the y direction and the first-floor exchanger along the x direction. This is a case that clearly demonstrates the problem, discussed in Section 6.1, of trying to compute a representative combined fragility curve by employing combination rules on the individual component fragilities. By inspecting Figure 7 it can be seen that the leftmost individual component fragilities intersect, especially for $AvgS_a$. This condition essentially renders the exchanger the most critical component for lower IMs, while the converters become critical at higher intensities. There is no straightforward combination rule to resolve such situations. Instead, the problem is fully resolved by defining the combined fragilities directly at the level of postprocessing the response history analysis results, i.e., by simultaneously checking at each IM the failure of the components assigned to each IC and identifying the attainment of the pertinent DSs.

Figures 8 and 9 present the empirical and the lognormally fitted combined component fragility curves for all buildings and DSs. Their medians and dispersions are listed in Table 9. In all cases, the evaluation of the fragilities by simultaneously checking across the same IC components for failure events, results in the fragilities being shifted to the left and to the dispersion being reduced for the majority of the cases, as opposed to the median and the dispersions that would have been obtained if the overall fragility was set equal to the fragility of the most critical component from each IC. Furthermore, as can be inferred from these figures and also the results tabulated in Table 9, with the sole exception of the RC3 building, the attainment of the most severe DS3 occurs prior to DS1–2. This is simply a testament to the existence of many IC III equipment items in each building that lead to early critical failures.

Interestingly, among all case study buildings, the most vulnerable is ST2. This is due to the period of its above-ground critical components (Table 2) being very close to the fundamental periods of the supporting structure (0.10–0.16sec), a condition that essentially implies (near) tuning of the first-floor acceleration-sensitive components and, consequently, high PCA demands. Again, this adverse effect should be considered by the designers, and when possible, it might be preferable to allocate the most critical component to lower storeys or the ground.

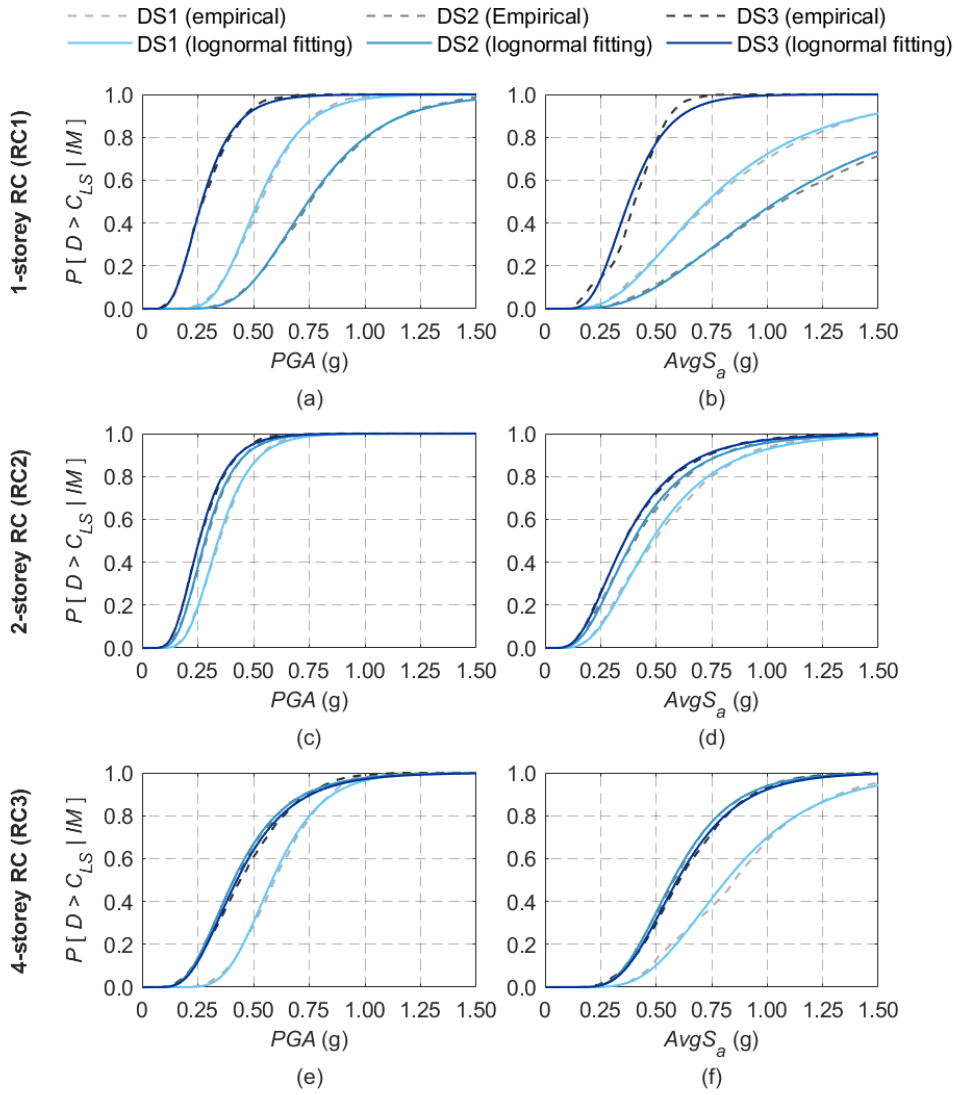

Figure 8. Combined component fragility curves for the considered RC1–3 assets.

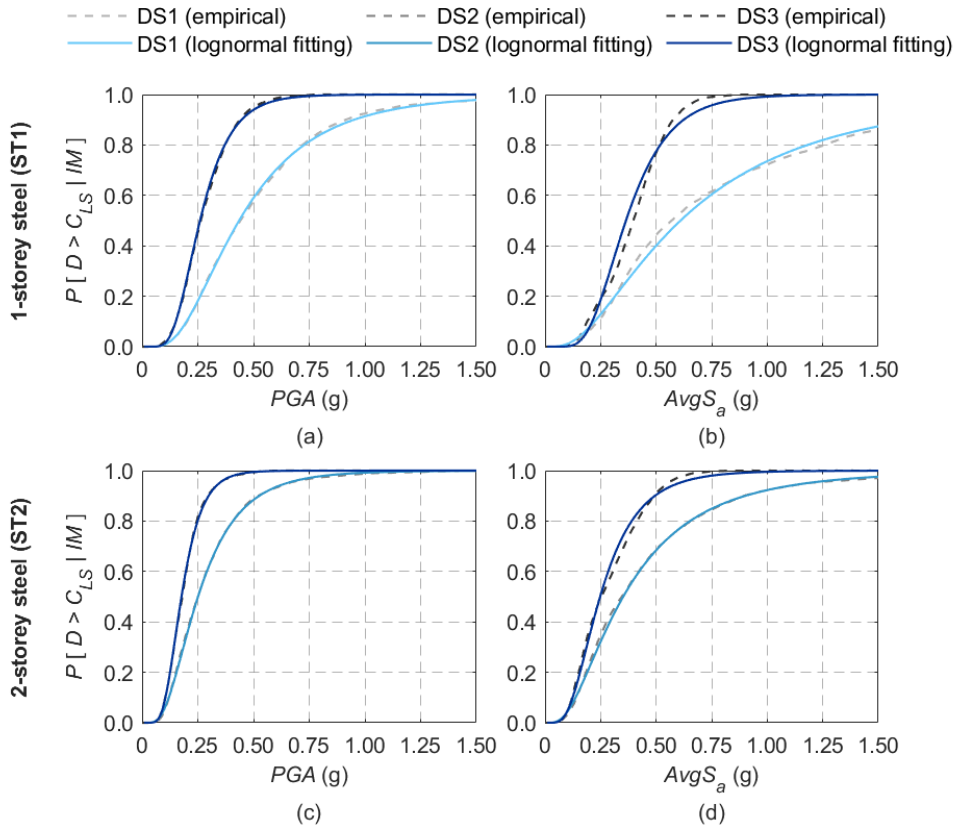

Figure 9. Combined component fragility curves for the considered ST1–2 assets.

Table 9: Median and dispersion of the combined component fragilities, to be used as overall fragilities for each building.

Damage States	PGA		$AvgS_a$	
	median (g)	dispersion	median (g)	dispersion
	1-storey RC (RC1)			
DS1	0.52	0.32	0.73	0.53
DS2	0.75	0.35	1.04	0.58
DS3	0.27	0.43	0.38	0.38
	2-storey RC (RC2)			
DS1	0.34	0.35	0.48	0.51
DS2	0.28	0.39	0.40	0.54
DS3	0.26	0.40	0.36	0.54
	4-storey RC (RC3)			
DS1	0.58	0.30	0.82	0.39
DS2	0.41	0.45	0.58	0.36
DS3	0.43	0.45	0.60	0.36
	1-storey steel (ST1)			
DS1	0.44	0.61	0.61	0.79
DS2	No components of IC II			
DS3	0.26	0.42	0.36	0.42
	2-storey steel (ST2)			
DS1	No components of IC I			
DS2	0.25	0.58	0.35	0.73
DS3	0.18	0.41	0.25	0.54

8 CONCLUSIONS

A seismic fragility analysis was undertaken for a set of open-frame buildings supporting essential process equipment that are typical to oil refineries. A step-by-step methodology is proposed for evaluating analytical fragility curves for equipment-supporting industrial structures. Several critical parameters, such as the model complexity and the definition of the IMs, were determined in view that the proposed framework will be eventually exploited to the seismic risk assessment of an entire plant. It was showcased that the seismic fragility of the supported acceleration-sensitive equipment is the one that drives the seismic performance of such assets and hence should be explicitly considered either in the design of new assets or the upgrade of existing ones. The adopted full probabilistic approach also revealed that the uncertainties associated with the amplification factor of floor acceleration demands are important and cannot be disregarded without potentially yielding unconservative fragility estimates. The resulting models, data, and framework can be exploited to stimulate further studies for managing the seismic risk in such critical infrastructure. The findings of this study hold for as long as (a) the main modelling assumptions for neglecting the component-structure interaction are being met; (b) the supporting structures are designed as per the strict design code regulations for industrial facilities and hence are characterised by significant overstrength; and (c) differential deformations among neighbouring buildings connected by piping are not a critical failure mode.

ACKNOWLEDGEMENTS

The authors would like to thank Ms. E. Vourlakou for preparing the photorealistic images of the buildings. We also acknowledge the comments made by the two anonymous reviewers who helped us improve the overall quality of this manuscript.

REFERENCES

ASCE/SEI (2017) Minimum design loads and associated criteria for buildings and other structures, ASCE/SEI 7-16. Structural Engineering Institute of American Society of Civil Engineers, Reston, Virginia. https://doi.org/10.1061/9780784414248

Astroza R, Pantoli E, Selva F, Restrepo JI, Hutchinson TC, Conte JP (2015) Experimental evaluation of a rooftop-mounted cooling tower. *Earthquake Spectra* 3(3): 1567–1589. https://doi.org/10.1193/071513EQS205M

Bakalis K, Karamanos SA (2021) Uplift mechanics of unanchored liquid storage tanks subjected to lateral earthquake loading. *Thin-Walled Structures* 158: 107145. https://doi.org/10.1016/j.tws.2020.107145

Bakalis K, Kohrangi M, Vamvatsikos D (2018) Seismic intensity measures for above-ground liquid storage tanks. *Earthquake Engineering and Structural Dynamics* 47(9): 1844–1863, 2018. https://doi.org/10.1002/eqe.3043

Bakalis K, Vamvatsikos D (2018) Seismic fragility functions via nonlinear response history analysis. *Journal of Structural Engineering (ASCE)* 144(10): 04018181. https://doi.org/10.1061/(ASCE)ST.1943-541X.0002141

Bakalis K, Vamvatsikos D, Fragiadakis M (2017) Seismic risk assessment of liquid storage tanks via a nonlinear surrogate model. *Earthquake Engineering and Structural Dynamics* 46(15): 2851–2868. https://doi.org/10.1002/eqe.2939

Baltzopoulos G, Baraschino R, Iervolino I (2019) On the number of records for structural risk estimation in PBEE. *Earthquake Engineering and Structural Dynamics* 48(5): 489–506. https://doi.org/10.1002/eqe.3145

Bi S, Kiaghadi A, Schulze BC, Bernier C, Bedient PB, Padgett JE, Rifai H, Griffin RJ (2021) Simulation of potential formation of atmospheric pollution from aboveground storage tank leakage after severe storms. *Atmospheric Environment* 248: 118225. https://doi.org/10.1016/j.atmosenv.2021.118225

Brennan AL, Koliou M (2020) Probabilistic loss assessment of a seismic retrofit technique for medium- and high-voltage transformer bushing systems in high seismicity regions. *Structure and Infrastructure Engineering*. https://doi.org/10.1080/15732479.2020.1785513

Bursi OS, Di Filippo R, La Salandra V, Pedot M, Reza MS (2018) Probabilistic seismic analysis of an LNG subplant. *Journal of Loss Prevention in the Process Industries* 53: 45–60. https://doi.org/10.1016/j.jlp.2017.10.009

Bursi OS, Reza MS, Abbiati G, Paolacci F (2015) Performance-based earthquake evaluation of a full-scale petrochemical piping system. *Journal of Loss Prevention in the Process Industries* 33: 10–22. https://doi.org/10.1016/j.jlp.2014.11.004

Butenweg C, Holtschoppen D (2013) Seismic design of industrial facilities in Germany, Proceedings of the International Conference on the Seismic Design of Industrial Facilities (SeDIF-Conference), Aachen, Germany. https://doi.org/10.1007/978-3-658-02810-7_6

Butenweg C. *et al*. (2020) Seismic performance of multiple-component systems in special risk industrial facilities, Proceedings of the 17th World Conference on Earthquake Engineering, Sendai, Japan.

Butenweg C. *et al*. (2021) Seismic performance of an industrial multi-storey frame structure with process equipment subjected to shake table testing. *Engineering Structures* 243: 112681. https://doi.org/10.1016/j.engstruct.2021.112681

Caprinozzi S, Dolšek M (2021) Seismic performance assessment of non-code-conforming and code-conforming supporting structures of elevated tanks using conventional and risk-based decision models. *Engineering Structures* 227: 111469. https://doi.org/10.1016/j.engstruct.2020.111469

CEN−European Committee for Standardization (2004) Eurocode 8: Design of structures for earthquake resistance. Part 1: General rules, seismic actions and rules for buildings. EN1998-1. Brussels, Belgium: CEN. https://eurocodes.jrc.ec.europa.eu/showpage.php?id=138

Cordova PP, Deierlein GG, Mehanny SS, Cornell CA (2000) Development of a two-parameter seismic intensity measure and probabilistic assessment procedure. Proceedings of the 2nd US–Japan Workshop on Performance-based Earthquake Engineering Methodology for RC Building Structures, Sapporo, Hokkaido.

Cornell CA, Jalayer F, Hamburger RO, Foutch DA (2002) The probabilistic basis for the 2000 SAC/FEMA steel moment frame guidelines. *Journal of Structural Engineering (ASCE)* 128(4): 526–533. https://doi.org/10.1061/(ASCE)0733-9445(2002)128:4(526)

Cornell CA, Krawinkler H (last accessed: February, 2022) Progress and challenges in seismic performance assessment. PEER Center News 2000. 3(2). https://apps.peer.berkeley.edu/news/2000spring/performance.html

D'Ayala D, Meslem A, Vamvatsikos D, Porter K, Rossetto T (2015) Guidelines for analytical vulnerability assessment of low/mid-rise buildings. GEM Technical Report, Vulnerability Global Component Project.

Diamanti K, Doukas I,Karamanos SA (2011) Seismic analysis and design of industrial pressure vessels. Proceedings of the 3rd International Conference on Computational Methods in Structural Dynamics and Earthquake Engineering (COMPDYN 2011), Corfu, Greece.

Di Sarno L, Karagiannakis G. (2020) On the seismic fragility of pipe rack–piping systems considering soil–structure interaction. *Bulletin of Earthquake Engineering* 18: 2723–2757. https://doi.org/10.1007/s10518-020-00797-0

Dymiotis C, Kappos AJ, Chryssanthopoulos MK (1999) Seismic reliability of RC frames with uncertain drift and member capacity. *Journal of Structural Engineering (ASCE)* 125(9):1038–1047. https://doi.org/10.1061/(ASCE)0733-9445(1999)125:9(1038)

Eads L, Miranda E, Lignos DG (2015) Average spectral acceleration as an intensity measure for collapse risk assessment. *Earthquake Engineering and Structural Dynamics* 44(12): 2057–2073. https://doi.org/10.1002/eqe.2575

Fahim MA, Elkilani E,Alsahlaf TA (2010) Fundamentals of petroleum refining (1st ed.). Amsterdam, The Netherlands: Elsevier. https://doi.org/10.1016/C2009-0-16348-1

Farhan M, Bousias S (2020) Seismic fragility analysis of LNG sub-plant accounting for component dynamic interaction. *Bulletin of Earthquake Engineering* 18: 5063–5085. https://doi.org/10.1007/s10518-020-00896-y

FEMA−Federal Emergency Management Agency (2003). Multi-hazard Loss Estimation Methodology, Earthquake Model. HAZUS-MH 2.1 Technical Manual. Washington, DC.

FEMA−Federal Emergency Management Agency (2018). Seismic performance assessment of buildings. Report FEMA P58-1. https://www.atcouncil.org/docman/fema/246-fema-p-58-1-seismic-performance-assessment-of-buildings-volume-1-methodology-second-edition/file

Franchin P, Petrini F, Mollaioli F (2018) Improved risk-targeted performance-based seismic design of reinforced concrete frame structures. *Earthquake Engineering and Structural Dynamics* 47(1): 49–67. https://doi.org/10.1002/eqe.2936

Fiore A, Rago C, Vanzi I, Greco R, Briseghella (2018) Seismic behavior of a low-rise horizontal cylindrical tank. *International Journal of Advanced Structural Engineering* 10:143–152. https://doi.org/10.1007/s40091-018-0188-y

Gillman TH, Le May I (2007) Mechanical and electrical failures leading to major fires. *Engineering Failure Analysis* 14(6 SPEC. ISS.): 995–1018. https://doi.org/10.1016/j.engfailanal.2006.11.049

Girgin S (2011) The natech events during the 17 August 1999 Kocaeli earthquake: aftermath and lessons learned. *Natural Hazards and Earth System Sciences* 11(4): 1129–1140. https://doi.org/10.5194/nhess-11-1129-2011

Girgin S, Necci A, Krausmann E (2019) Dealing with cascading multi-hazard risks in national risk assessment: The case of Natech accidents. International Journal of Disaster Risk Reduction 35: 101072. https://doi.org/10.1016/j.ijdrr.2019.101072

Godoy LA (2007) Performance of storage tanks in oil facilities damaged by hurricanes Katrina and Rita. *Journal of Performance of Constructed Facilities (ASCE)* 21(6): 441–449. https://doi.org/10.1061/(ASCE)0887-3828(2007)21:6(441)

Guo X, Zhang C (2019) Seismic fragility analysis of corroded chimney structures. *Journal of Performance of Constructed Facilities (ASCE)* 33(1): 04018087. https://doi.org/10.1061/(ASCE)CF.1943-5509.0001241

Hatayama K (2008) Lessons from the 2003 Tokachi-oki, Japan, earthquake for prediction of long-period strong ground motions and sloshing damage to oil storage tanks. *Journal of Seismology* 12: 255–263. https://doi.org/10.1007/s10950-007-9066-y

Hatayama K (2015) Damage to oil storage tanks from the 2011 Mw 9.0 Tohoku-Oki tsunami. *Earthquake Spectra* 31(2): 1103–1124. https://doi.org/10.1193/050713EQS120M

Hernandez-Hernandez D, Larkin T, Chouw N (2021) Evaluation of the adequacy of a spring-mass model in analyses of liquid sloshing in anchored storage tanks. *Earthquake Engineering and Structural Dynamics* 50(14): 3916–3935. https://doi.org/10.1002/eqe.3539

Iervolino I, Fabbrocino G, Manfredi G (2004) Fragility of standard industrial structures by a response surface based method. *Journal of Earthquake Engineering* 8(6): 927–945. https://doi.org/10.1142/S1363246904001717

Jalayer F, Cornell CA (2009) Alternative non-linear demand estimation methods for probability-based seismic assessments. *Earthquake Engineering and Structural Dynamics* 38(8): 951–972. https://doi.org/10.1002/eqe.876

Karakostas CZ, Moschonas IF, Lekidis VA, Papadopoulos SP (2015) Seismic performance of industrial pressure vessels: Parametric investigation of simplified modeling approaches for vulnerability assessment. Proceedings of the 5th International Conference on Computational Methods in Structural Dynamics and Earthquake Engineering (COMPDYN 2015), Athens, Greece. https://doi.org/10.7712/120115.3520.944

Kazantzi AK, Righiniotis TD, Chryssanthopoulos MK (2008) Fragility and hazard analysis of a welded steel moment resisting frame. *Journal of Earthquake Engineering* 12(4): 596–615. https://doi.org/10.1080/13632460701512993

Kazantzi AK, Righiniotis TD, Chryssanthopoulos MK (2011) A simplified fragility methodology for regular steel MRFs. *Journal of Earthquake Engineering* 15(3): 390–403. https://doi.org/10.1080/13632469.2010.498559

Kazantzi AK, Vamvatsikos D (2015) Intensity measure selection for vulnerability studies of building classes. *Earthquake Engineering and Structural Dynamics* 44(15): 2677–2694. https://doi.org/10.1002/eqe.2603

Kazantzi AK, Vamvatsikos D, Lignos D (2014) Seismic performance of a steel moment-resisting frame subject to strength and ductility uncertainty. *Engineering Structures* 78: 69–77. https://doi.org/10.1016/j.engstruct.2014.06.044

Kazantzi AK, Vamvatsikos D, Miranda E (2020) Evaluation of seismic acceleration demands on building non-structural elements. *Journal of Structural Engineering (ASCE)* 146(7): 04020118. https://doi.org/10.1061/(ASCE)ST.1943-541X.0002676

Kazantzi AK, Vamvatsikos D (2021) Practical performance-based design of friction pendulum bearings for a seismically isolated steel top story spanning two RC towers. *Bulletin of Earthquake Engineering* 19: 1231–1248. https://doi.org/10.1007/s10518-020-01011-x

Khan FI, Amyotte PR (2007) Modeling of BP Texas City refinery incident. *Journal of Loss Prevention in the Process Industries* 20(4–6): 387–395. https://doi.org/10.1016/j.jlp.2007.04.037

Kohrangi M, Bazzurro P, Vamvatsikos D, Spillatura A (2017) Conditional spectrum-based ground motion record selection using average spectral acceleration. *Earthquake Engineering & Structural Dynamics* 46(10): 1667–1685. https://doi.org/10.1002/eqe.2876

Kohrangi M, Vamvatsikos D, Bazzurro P (2020) Multi-level conditional spectrum-based record selection for IDA. *Earthquake Spectra* 36(4): 1976–1994. https://doi.org/10.1177/8755293020919425

Korndörfer J, Hoffmeister B, Feldmann M (2017) Seismic fragility of horizontal pressure vessels - Effects of structural interaction between industrial components. Proceedings of the 6th International Conference on Computational Methods in Structural Dynamics and Earthquake Engineering (COMPDYN 2017), 3102–3111, Rhodes, Greece. https://doi.org/10.7712/120117.5630.18148

Krausmann E, Cruz AM (2021) Natech risk management in Japan after Fukushima – What have we learned? *Loss Prevention Bulletin* 277. https://www.icheme.org/media/15301/krausmannnew.pdf

Kwon OS, Elnashai A (2006) The effect of material and ground motion uncertainty on the seismic vulnerability curves of RC structure. *Engineering Structures* 28(2): 289–303. https://doi.org/10.1016/j.engstruct.2005.07.010

Lin T, Haselton CB, Baker JW (2013) Conditional spectrum-based ground motion selection. Part I: Hazard consistency for risk-based assessments. *Earthquake Engineering and Structural Dynamics* 42(12): 1847–1865. https://doi.org/10.1002/eqe.2301

McKenna F, Fenves GL (2001) The OpenSees Command Language Manual (1.2 edn). University of California Berkeley, Berkeley, CA.

Melchers RE, Beck AT (2017) *Structural reliability analysis and prediction* (3rd edition). John Wiley & Sons. https://doi.org/10.1002/9781119266105

Melissianos VE, Karaferis ND, Kazantzi AK, Bakalis K, Vamvatsikos D (2022) An integrated model for the seismic risk assessment of an oil refinery. 3rd International Conference on Natural Hazards & Infrastructure (ICONHIC), Athens, Greece.

Merino Vela RJ, Brunesi E, Nascimbene R (2019) Seismic assessment of an industrial frame-tank system: development of fragility functions. *Bulletin of Earthquake Engineering* 17: 2569–2602. https://doi.org/10.1007/s10518-018-00548-2

Patkas LA, Karamanos SA (2007) Variational solutions for externally induced sloshing in horizontal-cylindrical and spherical vessels. *Journal of Engineering Mechanics (ASCE)* 133(6): 641–655. https://doi.org/10.1061/(ASCE)0733-9399(2007)133:6(641)

Phan HN, Paolacci F, Di Filippo R, Bursi OS (2020) Seismic vulnerability of above-ground storage tanks with unanchored support conditions for Na-tech risks based on Gaussian process regression. *Bulletin of Earthquake Engineering* 18: 6883–6906. https://doi.org/10.1007/s10518-020-00960-7

Pulkkinen U (1993) Methods for combination of experts judgements. *Reliability Engineering and System Safety* 111–118: 40. https://doi.org/10.1016/0951-8320(93)90101-4

Sezen H, Whittaker AS (2006) Seismic performance of industrial facilities affected by the 1999 Turkey Earthquake. *Journal of Performance of Constructed Facilities (ASCE)* 20(1): 28–36. https://doi.org/10.1061/(ASCE)0887-3828(2006)20:1(28)

Spritzer JM, Guzey S (2017) Review of API 650 Annex E: Design of large steel welded aboveground storage tanks excited by seismic loads. *Thin-Walled Structures* 112: 41–65. https://doi.org/10.1016/j.tws.2016.11.013

Sullivan D, Metro S, Pujadó PR (2015) Handbook of petroleum processing. (S. A. Treese, P. R. Pujadó, and D. S. J. Jones, Eds.) Cham, Switzerland: Springer International Publishing. https://doi.org/10.1007/978-3-319-14529-7

Taghavi S, Miranda E (2008) Effect of interaction between primary and secondary systems on floor response spectra. Proceedings of the 14th World Conference on Earthquake Engineering, Beijing, China.

Tsantaki S, Adam C, Ibarra LF (2017) Intensity measures that reduce collapse capacity dispersion of P-delta vulnerable simple systems. *Bulletin of Earthquake Engineering* 15(3): 1085–109. https://doi.org/10.1007/s10518-016-9994-4

Vamvatsikos D, Cornell CA (2002) Incremental dynamic analysis. *Earthquake Engineering and Structural Dynamics* 31(3): 491–514. https://doi.org/10.1002/eqe.141

Vamvatsikos D, Cornell CA (2004) Applied incremental dynamic analysis. *Earthquake Spectra* 20(2): 523–553. https://doi.org/10.1193/1.1737737

Vamvatsikos D, Cornell CA (2005) Developing efficient scalar and vector intensity measures for IDA capacity estimation by incorporating elastic spectral shape information. *Earthquake Engineering and Structural Dynamics* 34(13): 1573–1600. https://doi.org/10.1002/eqe.496

Vamvatsikos D, Bakalis K, Kohrangi M, Pyrza S, Castiglioni C, Kanyilmaz A, Morelli F, Stratan A, D' Aniello M, Calado L, Proença JM, Degee H, Hoffmeister B, Pinkawa M, Thanopoulos P, Vayas I (2020) A risk-consistent approach to determine EN1998 behaviour factors for lateral load resisting systems. *Soil Dynamics and Earthquake Engineering* 131: 106008. https://doi.org/10.1016/j.soildyn.2019.106008

Vathi M, Karamanos SA, Kapogiannis IA, Spiliopoulos KV (2017) Performance Criteria for Liquid Storage Tanks and Piping Systems Subjected to Seismic Loading. *Journal of Pressure Vessel Technology (ASME)* 139(5): 051801. https://doi.org/10.1115/1.4036916

Watkins D, Chui L, Hutchinson T, Hoehler MS (2009) Survey and characterization of floor and wall mounted mechanical and electrical equipment in buildings. Structural systems research project report SSRP 09/11, Department of Structural Engineering, University of California San Diego, La Jolla, CA.

Wieschollek M, Hoffmeister B, Feldmann M (2013) Experimental and numerical investigations on nozzle reinforcements. Proceedings of the ASME 2013 Pressure Vessels & Piping Division Conference, ASME, Paris, France, PVP2013-97430. https://doi.org/10.1115/PVP2013-97430

Yu C-C, Whittaker AS (2021) Review of analytical studies on seismic fluid-structure interaction of base-supported cylindrical tanks. *Engineering Structures* 233: 111589. https://doi.org/10.1016/j.engstruct.2020.111589

Zhang Z, Park J, Kwon O-S, Sextos A, Strepelias E, Stathas N, Bousias S (2021) Hybrid simulation of structure-pipe-structure interaction within a gas processing plant. *Journal of Pipeline Systems Engineering and Practice (ASCE)* 12(2): 04020073. https://doi.org/10.1061/(ASCE)PS.1949-1204.0000526

STATEMENTS AND DECLARATIONS

Funding

This research has been co-financed by the European Union through the Horizon 2020 research and innovation programmes "INFRASTRESS–Improving resilience of sensitive industrial plants & infrastructures exposed to cyber-physical threats, by means of an open testbed stress-testing system" under Grant Agreement No. 833088, and "HYPERION–Development of a decision support system for improved resilience & sustainable reconstruction of historic areas to cope with climate change & extreme events based on novel sensors and modelling tools" under Grant Agreement No. 821054.

Competing Interests

The authors have no relevant financial or non-financial interests to disclose.

Data Availability

Some or all data, models, or code that support the findings of this study are available from the corresponding author upon reasonable request.